Coastal Engineering 117 (2016) 57–69

Contents lists available at ScienceDirect

Coastal Engineering

journal homepage: www.elsevier.com/locate/coastaleng

Wave-averaged properties in a submerged canopy: Energy density, energy flux, radiation stresses and Stokes drift

Niels G. Jacobsen

Coastal Structures and Waves, Deltares, Boussinesqweg 1, Delft 2629 HV, The Netherlands

ARTICLE INFO

Article history:
Received 17 March 2016
Received in revised form 6 July 2016
Accepted 23 July 2016
Available online 4 August 2016

Keywords:
Submerged vegetation
Wave theory
Wave energy density
Wave energy flux
Vegetated group velocity
Radiation stresses
Stokes drift

ABSTRACT

This work analyses basic wave properties originating from the interaction between waves and submerged rigid vegetation. First of all, an analytical framework is presented that describes the propagation and dissipation of waves over a rigid and submerged canopy, where the flow resistance is linearised. A nonlinear closure term is introduced to ensure that the work done by the linearised flow resistance equals that of the nonlinear flow resistance. The anisotropic flow resistance is found to have an impact on both the distribution of velocities and pressure inside the canopy and it partly explains the small decrease in flow velocities inside the canopy, which was previously observed experimentally.

The following second order wave properties are derived: the wave energy density, the wave energy flux, the vegetated group velocity of the wave energy density, the radiation stress components parallel and perpendicular to the direction of wave propagation, the Eulerian and Lagrangian Stokes velocities and fluxes. The additional Stokes drift due to the discontinuity in the velocity field at the top of the vegetation is derived; the inclusion of this mass flux in the Lagrangian formulation of the Stokes drift is important for the ratio between the Lagrangian and Eulerian Stokes drifts.

The relation between the wave energy density and the wave energy flux, i.e. the vegetated group velocity of the wave energy density, is of practical importance for large scale wave modelling. The modification to the vegetated group velocity relative to that derived from linear wave theory on non-dissipative waves is described. It is seen that the corrections to linear wave theory are of H^{γ}, where γ is in the interval 1.5–2.0.

1. Introduction

This work was initially inspired by some previous research efforts. First of all, Döbken (2015) showed with the help of a simple 1DV numeric model (Uittenbogaard and Klopman, 2001; Dijkstra and Uittenbogaard, 2010) that the vertical distribution of the Lagrangian Stokes drift velocity in the presence of vegetation differs from that of non-dissipative linear wave theory. The most prominent discrepancy was the local maximum of the Stokes drift velocity adjacent to the top of the canopy, which was caused by the local and large vertical gradient in the horizontal velocity.

Furthermore, (Luhar et al., 2010; Van Rooijen et al., 2016) utilised expressions for the Stokes drift in discussions of the mean flow properties inside a canopy and for the numerical modelling of the wave-induced mean setup inside the Generalised Lagrangian Mean framework (Andrews and McIntyre, 1978). These works relied on a magnitude of the Stokes drift obtained from non-dissipative, linear wave theory.

These combined research efforts led the author to ask the questions: (i) Is it possible to derive an analytical expression for the Lagrangian Stokes drift that also has a local maximum around the top of the canopy? (ii) Based on these results, can it be stated that the Stokes drift is of the same magnitude with and without the presence of vegetation? These questions will be answered in the following.

With an analytical solution at hand, it was straightforward to extend the analysis to additional second order wave properties. The derivation and application of an expression for the radiation stress component in the direction of wave propagation was already reported in Mendez et al. (1998), which is the reason that the focus in the present work is given to the wave energy density, the wave energy flux and the related vegetated group velocity.

Large scale numerical modelling of the interaction between waves and vegetation is conducted over several decades (Dalrymple et al., 1984; Mendez and Losada, 2004; Suzuki et al., 2011; Cao et al., 2015; Van Rooijen et al., 2016). These works cover methods such as the mild slope equations and the wave action equations with

E-mail address: niels.jacobsen@deltares.nl (N.G. Jacobsen).

http://dx.doi.org/10.1016/j.coastaleng.2016.07.009
0378-3839/

the common feature that the vegetated group velocity for the wave energy density is set equal to the group velocity:

$$c_g = \frac{1}{2}\frac{\sigma}{k_{\alpha=1}}\left(1+\frac{2k_{\alpha=1}h}{\sinh 2k_{\alpha=1}h}\right) \tag{1}$$

where $k_{\alpha=1}$ is the wave number, σ is the cyclic frequency and h is the total water depth. The relationship between $k_{\alpha=1}$ and σ is given through the linear dispersion relation for a water depth of h (see Eq. (20) below). α is defined below.

Gu and Wang (1991) saw that the general wave number over a permeable sea bed with isotropic resistance differs from $k_{\alpha=1}$. Consequently, it is natural to ask the following: Since the wave number is a function of the resistance properties of vegetation or a permeable sea bed, will the transport of the wave energy density still be conducted with the group velocity c_g? This leads to related questions concerning the influence of the vegetation on the wave energy density and the wave energy flux. These questions will be addressed in the following.

It is noted that analytical solutions to wave propagation over permeable layers and vegetation were presented previously (Liu and Dalrymple, 1984; Gu and Wang, 1991; Méndez et al., 1999, to name some), but except for the brief outline in Mendez et al. (1998), the second order (wave-averaged) wave properties do not seem to have been given any attention. The same mathematical approach was applied in the works mentioned above for both permeable bed and vegetated fields. It means that the present work is not exclusively limited to vegetated fields, but is also relevant for submerged, permeable breakwaters or permeable natural reefs.

The outline of the present work is as follows. In Section 2 the mathematical framework is presented and the handling of the dissipation due to an anisotropic resistance term is described. A simple validation against experimental data is presented in Section 2.5. In Section 4 the vertical variation of velocities and pressure is discussed along with an example of the phase lags between the horizontal and vertical velocity components. In Section 5 expressions for the wave energy density, wave energy flux and vegetated group velocity are derived and quantified as functions of wave and canopy properties. The radiation stress components along and perpendicular to the direction of wave propagation are presented in Section 6. The horizontal Stokes drift is evaluated in both Eulerian and Lagrangian frameworks in Section 7 and the vertical Stokes velocity at the free surface is utilised to link the Eulerian and Lagrangian expressions. The paper is finalised with a discussion and a conclusion.

2. Mathematical description

The local behaviour of a non-breaking wave field in a canopy consisting of rigid, submerged vegetation is described in this section. The term local means that effects of the finite length of the canopy will not be covered here. A finite length was included in the work by Méndez et al. (1999), and their solution resulted in an expression for the degree of reflection due to the presence of the canopy (though not explicitly analysed). This came with a considerable increase in the complexity of the mathematical description, since evanescence modes were required to match the solution at the ends of the canopy. Consequently, the effects of reflected waves and evanescence modes are omitted in this work. The omission of the evanescence modes are acceptable, since they decay exponentially away from the ends of the canopy (Méndez et al., 1999). The reflected wave is omitted in this work, because the reflection coefficient is assumed small and only second order properties in the wave height are analysed in this work.

Furthermore, boundary layer effects on top of the vegetation field and at the bottom are assumed to be negligible in terms of the wave dissipation. Consequently, these boundary layers will be excluded in this mathematical treatment. Findings by Liu and Dalrymple (1984) for percolation in permeable beds showed that the dissipation due to boundary layers is small in comparison to the dissipation by the permeable medium. This finding is also assumed to hold for dissipation in a submerged canopy.

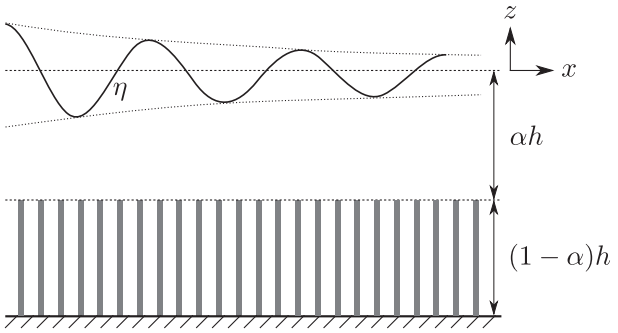

Fig. 1. Sketch of the physical problem of wave propagation and wave attenuation over rigid, submerged vegetation.

Rigid vegetation is not the only type of vegetation, but inclusion of flexibility would greatly increase the complexity of the mathematical derivations. Furthermore, the concept of *effective length* of the vegetation as discussed by Luhar and Nepf (2016) points in the direction of an engineering treatment of the vegetation as stiff elements. The validity of the assumptions will be discussed in Section 8.1.

In the following a vector notation will be used for a matter of compactness of the equations, while a scalar form is used in the subsequent sections. Therefore, the two-dimensional velocity vector is defined as $\mathbf{u} = [u; w]$ and the two-dimensional Cartesian coordinate as $\mathbf{x} = [x; z]$. Lowercase, bold symbols refer to vector properties and uppercase, bold symbols refer to tensors properties of rank 2.

2.1. Definition of the mathematical framework

A sketch of the physical system is presented in Fig. 1. The mathematical derivation will loosely follow the ideas in Gu and Wang (1991), Méndez et al. (1999). Only submerged vegetation will be analysed in this work, consequently $0 < \alpha$.

The wave motion is described by the velocity potential Φ above the canopy, where the velocity field is assumed irrotational and incompressible, i.e. the solution to Φ is given by the Laplace equation:

$$\nabla^2\Phi = 0 \quad \text{for} -\alpha h \le z \le 0 \tag{2}$$

The velocity field above the canopy is given as $\mathbf{u} = \nabla\Phi$.

The flow inside the canopy is described by the linearised momentum equation based on filter velocities (see e.g. Jensen et al., 2014):

$$\begin{aligned}\frac{\partial}{\partial t}\frac{\mathbf{u}}{n} &= -\frac{1}{\rho}\nabla p - \mathbf{C}_m\frac{\partial}{\partial t}\frac{\mathbf{u}}{n} - \mathbf{B}\mathbf{u}\|\mathbf{u}\|_2 \\ &\simeq -\frac{1}{\rho}\nabla p - \mathbf{C}_m\frac{\partial}{\partial t}\frac{\mathbf{u}}{n} - \mathbf{F}\mathbf{u}\end{aligned} \tag{3}$$

The second approximation is a linearisation of the nonlinear resistance term as suggested by Sollitt and Cross (1972). The evaluation of the real-valued friction tensor $\mathbf{F}$ is described in Section 2.3. In Eq. (3), $\mathbf{u}$ is the Eulerian filter velocity vector, n is the porosity, t is time, ρ is the uniform density of water, p is the pressure in excess of the hydrostatic, $\mathbf{C}_m$ is the added mass tensor and $\mathbf{B}$ is the resistance tensor for the quadratic flow resistance. Assuming that $\mathbf{u}$ is periodic in time

with the cyclic frequency σ, the following (linearised) expression for the pressure inside the canopy is obtained:

$$-\frac{1}{\rho}\nabla p = \left[\frac{1}{n}\left(1+\mathbf{C}_m\right)\sigma i + \mathbf{F}\right]\mathbf{u} = \mathbf{R}\mathbf{u} \tag{4}$$

Here, $i = \sqrt{-1}$ is the complex number and $\mathbf{R}$ is the bulk resistance tensor:

$$\mathbf{R} = \begin{bmatrix} r_x & 0 \\ 0 & r_z \end{bmatrix} \tag{5}$$

The resistance tensors $\mathbf{C}_m$ and $\mathbf{B}$ are defined as

$$\mathbf{C}_m = NA\begin{bmatrix} c_{mx} & 0 \\ 0 & c_{mz} \end{bmatrix} \quad \text{and} \quad \mathbf{B} = \frac{1}{2}Nd\begin{bmatrix} c_{Dx} & 0 \\ 0 & c_{Dz} \end{bmatrix} \tag{6}$$

Here, c_{mx}, c_{mz}, c_{Dx} and c_{Dz} are inertia and drag coefficients along the x and z axes and they introduce a possible anisotropy to the resistance term. N is the number of stems per square meters, A is the horizontal cross section area of the stems and d is the stem diameter. In the case of rigid (and vertical) vegetation it is reasonable to assume that $c_{mz} \simeq 0$ and $c_{Dz} \simeq 0$, i.e. $|r_z| < |r_x|$. Here $|\cdot|$ is the modulus operator on a complex number. Different cross section geometry of the (vertically uniform) vegetation can be introduced through the formulation of $\mathbf{C}_m$ and $\mathbf{B}$.

The use of the continuity equation ($\nabla\cdot\mathbf{u} = 0$) on Eq. (4) results in a partial differential equation for the in-canopy pressure field:

$$\nabla\cdot r_x\mathbf{R}^{-1}\nabla p = 0 \quad \text{for} \quad -h \le z \le -\alpha h \tag{7}$$

The bottom boundary condition for p is that the bottom is impermeable, i.e.

$$\frac{1}{\rho}\frac{\partial p}{\partial z} = -r_z w = 0 \quad \text{for} \quad z = -h \tag{8}$$

The classical boundary conditions hold for the free surface:

$$\eta = -\frac{1}{g}\frac{\partial \Phi}{\partial t} \quad \text{for} \quad z = 0 \tag{9}$$

$$\frac{\partial \Phi}{\partial z} = -\frac{1}{g}\frac{\partial^2 \Phi}{\partial t^2} \quad \text{for} \quad z = 0 \tag{10}$$

Here, $\eta = H/2\exp\left(i(\sigma t - kx)\right)$ is the free surface elevation, where H is the wave height at $x = 0$ and the wave number is complex: $k = k_r + ik_i$. The sub-indices r and i refer to the real and imaginary parts respectively. The definition of the argument $i(\sigma t - kx)$ means that $0 < k_r$ and $k_i \le 0$ for a wave propagating along the positive x-axis.

It is enforced that the vertical velocity matches at the interface between the two regions:

$$-\frac{1}{\rho r_z}\frac{\partial p}{\partial z} = \frac{\partial \Phi}{\partial z} \quad \text{for} \quad z = -\alpha h \tag{11}$$

Note that Méndez et al. (1999) introduced a scaling of porosity, because they used the pore velocity field inside the canopy in their derivations.

The second matching boundary condition is that the pressure is continuous across the top of the vegetation:

$$\frac{p}{\rho} = -\frac{\partial \Phi}{\partial t} \quad \text{for} \quad z = -\alpha h \tag{12}$$

This means there is no boundary condition that enforces a matching of the horizontal velocity, thus a finite jump in the horizontal velocity is to be expected. This is consistent with previous works on potential wave theory and it originates from the omission of the boundary layer effects around the top of the vegetation (Liu and Dalrymple, 1984).

2.2. The solution

The shape of the solutions to the two regions are assumed as follows:

$$\Phi = \left[A\cosh k(\alpha h + z) + B\sinh k(\alpha h + z)\right]e^{i(\sigma t - kx)} \tag{13}$$

and

$$\frac{p}{\rho} = D\cosh\kappa(h+z)e^{i(\sigma t - kx)} \tag{14}$$

A, B and D are coefficients, k is the wave number and κ is a shape function for the vertical variation of the pressure inside the canopy. The argument $k(\alpha h + z)$ in Eq. (13) makes the derivation of the closure coefficients easier than other choices of the argument, i.e. $k(h+z)$ (Gu and Wang, 1991). It is observed that Eq. (14) directly fulfills the boundary condition in Eq. (8). Inserting Eq. (14) into Eq. (7) yields the following relationship:

$$k^2 = \frac{r_x}{r_z}\kappa^2 = \frac{r_x r_z^*}{|r_z|^2}\kappa^2 \tag{15}$$

where it is noted that $|\kappa| \le |k|$ for the present application. The equality holds in the special case of no vegetation or isotropic resistance. * denotes the complex conjugate.

Insertion of the assumed shape for Φ and p into the matching conditions (Eqs. (11) and (12)) yields

$$A = i\frac{\cosh\kappa h(1-\alpha)}{\sigma}D \tag{16}$$

and

$$B = -\frac{1}{r_z}\frac{\kappa\sinh\kappa h(1-\alpha)}{k}D \tag{17}$$

The free surface boundary conditions yield an expression for D and the modified dispersion relation in the presence of vegetation (see also Gu and Wang, 1991, for the case of isotropic resistance). D is given as

$$D = \frac{gH}{2}\frac{\left[1 + \frac{\sigma i}{r_z}\frac{\kappa}{k}\tanh\kappa h(1-\alpha)\tanh\alpha kh\right]^{-1}}{\cosh\kappa h(1-\alpha)\cosh\alpha kh} \tag{18}$$

The dispersion relation reads:

$$\sigma^2 - gk\tanh\alpha kh = \frac{i\sigma\kappa}{r_z k}\tanh\kappa h(1-\alpha)\left[gk - \sigma^2\tanh\alpha kh\right] \tag{19}$$

In the limit of vanishing flow resistance ($r_x = r_z = i\sigma$) the dispersion relation Eq. (19) reduces to the linear dispersion relation:

$$\sigma^2 = gk\tanh kh \tag{20}$$

for any value of α.

The evaluation of the linearised resistance tensor $\mathbf{F}$ will be discussed in the following section, but it is worthwhile to note that $\mathbf{F}$ is

based on a nonlinear matching of the work done by the vegetation due to the two resistance terms **Fu** (linear) and **Bu**$\|\mathbf{u}\|_2$ (nonlinear). This means that the magnitude of **F**, amongst others, becomes a function of the wave height, H. Consequently, the first order solution to the wave propagation in a rigid, submerged canopy is amplitude dispersive due to a nonlinear closure. Amplitude dispersion only appears as a third order contribution in the classical Stokes perturbation solutions for non-dissipative waves (Madsen and Schäffer, 1998).

2.3. Equivalent resistance coefficient

The equivalent (real-valued) resistant coefficients in $\mathbf{F} = [f_x 0; 0 f_z]$ are defined such that the linearised work done on the vegetation over one wave period is identical to the work done by the nonlinear resistance formulation, see Sollitt and Cross (1972). This approach is used as a standard approach for the analytical description of interaction between waves and permeable structures (Madsen, 1983; Dalrymple et al., 1991) and also utilised in the analytical work for the interaction between waves and vegetation fields (Asano et al., 1992; Méndez et al., 1999).

Consequently, **F** is found from the following equality:

$$\overline{\int_{-h}^{-\alpha h} \mathrm{Re}[\mathbf{u}]^T(\mathbf{B}\mathrm{Re}[\mathbf{u}]\|\mathrm{Re}[\mathbf{u}]\|_2)\mathrm{d}z} = \overline{\int_{-h}^{-\alpha h} \mathrm{Re}[\mathbf{u}]^T(\mathbf{F}\mathrm{Re}[\mathbf{u}])\mathrm{d}z} \tag{21}$$

Here, the overbar means period averaging.

Eq. (21) contains diagonal components f_x and f_z in **F** as unknowns, but since the flow resistance in the vertical direction will be assumed negligible ($f_z = 0$), the equivalent quadratic resistance coefficient in the horizontal direction (f_x) is straightforward to evaluate through an iterative solution procedure similar to the one outlined in Madsen (1983).

Note that this closure introduces a higher order effect into the solution, therefore the solution will be amplitude dispersive at lowest order.

2.4. Definitions

A couple of definitions are introduced below to obtain simpler expressions in the following sections; recall that the velocity vector is given as $\mathbf{u} = [u; w]$. First, the primary variables above the vegetation ($-\alpha h \le z \le 0$) read:

$$\begin{aligned} u_+ &= U_+ e^{i\theta} \\ &= -ik\left[A\cosh k(\alpha h + z) + B\sinh k(\alpha h + z)\right] e^{i\theta} \end{aligned} \tag{22}$$

$$\begin{aligned} w_+ &= W_+ e^{i\theta} \\ &= k\left[A\sinh k(\alpha h + z) + B\cosh k(\alpha h + z)\right] e^{i\theta} \end{aligned} \tag{23}$$

$$\begin{aligned} p_+ &= P_+ e^{i\theta} \\ &= -i\sigma\left[A\cosh k(\alpha h + z) + B\sinh k(\alpha h + z)\right] e^{i\theta} \end{aligned} \tag{24}$$

where $\theta = \sigma t - kx$. Inside the canopy the primary variables read:

$$u_- = U_- e^{i\theta} = \frac{ik}{r_x} D\cosh\kappa(h + z)e^{i\theta} \tag{25}$$

$$w_- = W_- e^{i\theta} = -\frac{\kappa}{r_z} D\sinh\kappa(h + z)e^{i\theta} \tag{26}$$

$$p_- = P_- e^{i\theta} = D\cosh\kappa(h + z)e^{i\theta} \tag{27}$$

The sub-indices + and − will throughout the remainder of this text refer to properties above or inside the canopy respectively. Omission of the sub-index refers to both regions.

The integration over the vertical is needed to analyse the various period averaged and depth integrated quantities. The following integrals are defined above the canopy:

$$\begin{aligned} C_{1,+} &= \int_{-\alpha h}^{0} \cosh k(\alpha h + z)\cosh^* k(\alpha h + z)\mathrm{d}z \\ &= \frac{1}{4k_r k_i}\left[k_r \sin 2k_i \alpha h + k_i \sinh 2k_r \alpha h\right] \end{aligned} \tag{28}$$

Here, $k = k_r + ik_i$ and $\cosh^*$ refers to the complex conjugate of the cosine hyperbolic. Similarly three additional integrals are defined above the canopy:

$$\begin{aligned} C_{2,+} &= \int_{-\alpha h}^{0} \sinh k(\alpha h + z)\sinh^* k(\alpha h + z)\mathrm{d}z \\ &= \frac{1}{4k_r k_i}\left[k_i \sinh 2k_r \alpha h - k_r \sin 2k_i \alpha h\right] \end{aligned} \tag{29}$$

$$\begin{aligned} C_{3,+} &= \int_{-\alpha h}^{0} \cosh k(\alpha h + z)\sinh^* k(\alpha h + z)\mathrm{d}z \\ &= \frac{1}{4k_r k_i}\left[k_i(\cosh 2k_r \alpha h - 1) + ik_r(\cos 2k_i \alpha h - 1)\right] \end{aligned} \tag{30}$$

$$C_{4,+} = \int_{-\alpha h}^{0} \sinh k(\alpha h + z)\cosh^* k(\alpha h + z)\mathrm{d}z = C_{3,+}^* \tag{31}$$

Inside the canopy, the following two integrals are defined:

$$\begin{aligned} C_{1,-} &= \int_{-h}^{-\alpha h} \cosh\kappa(h + z)\cosh^*\kappa(h + z)\mathrm{d}z \\ &= \frac{1}{4\kappa_r \kappa_i}\left[\kappa_r \sin 2\kappa_i(1 - \alpha)h + \kappa_i \sinh 2\kappa_r(1 - \alpha)h\right] \end{aligned} \tag{32}$$

$$\begin{aligned} C_{2,-} &= \int_{-h}^{-\alpha h} \sinh\kappa(h + z)\sinh^*\kappa(h + z)\mathrm{d}z \\ &= \frac{1}{4\kappa_r \kappa_i}\left[\kappa_i \sinh 2\kappa_r(1 - \alpha)h - \kappa_r \sin 2\kappa_i(1 - \alpha)h\right] \end{aligned} \tag{33}$$

2.5. Basic validation

Sánchez-González et al. (2011) performed a large number of experimental studies on the wave attenuation over a canopy that represents the species *Posidonia oceanica*. The canopy was 9 m long and had a vegetation density of 40,000 stems/m^2. Each stem was 0.1 m long and the cross section measured 3 mm × 0.1 mm. This yielded a porosity of 0.98 inside the canopy. In this basic validation four of their tests with a water depth of 0.3 m and a regular wave period of 1.25 s are compared with the experimental results.

The resistance coefficients are set to $c_{mx} = c_{mz} = c_{Dz} = 0$. In works with permeable, coastal structures the added mass coefficient is typically written as (Van Gent, 1995):

$$c_{mx} = \gamma\frac{1 - n}{n} \tag{34}$$

Here $\gamma = 0.34$ was used. Therefore, $c_{mx} = 0.004$; thus it can safely be neglected. Further, it is estimated that the Keulegan–Carpenter

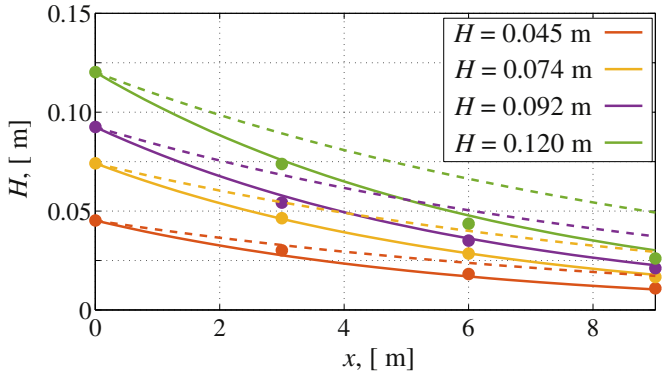

Fig. 2. A comparison between the analytical model and the experimental data by Sánchez-González et al. (2011). Full line: Including the correction factor of 1.7. Dashed line: Without the correction factor.

number is in the order of 50 or larger, thus the forces on the vegetation are drag-dominated (Sumer and Fredsøe, 1999).

The expression for the drag coefficient derived by Sánchez–González et al. (2011) was used, which reads

$$\tilde{c}_{Dx} = \frac{22.9}{KC^{1.09}} \quad \text{where} \quad KC = \frac{u_\alpha T}{b} \tag{35}$$

Here, KC is the Keulegan–Carpenter number, u_α is the velocity at the top of the canopy based on non-dissipative linear wave theory, and $b = 3.0$ mm is the dimension of the vegetation. $\tilde{c}_{Dx}$ in Sánchez–González et al. (2011) is derived based on linear wave theory without the presence of vegetation, i.e. the velocities will be smaller with the present theory and it must be expected that $\tilde{c}_{Dx} < c_{Dx}$. In the present case, a constant and ad-hoc scaling factor of 1.7 has been applied to all four cases. Whether this scaling factor is generally applicable has not been investigated.

The results are shown in Fig. 2 and it is seen that for all four wave heights, the theoretical model reproduces the experimental data. It should be noted that the decay is based on the wave properties at $x = 0$ m, i.e. the effect of the gradual decay of the wave height, and thus the rate of dissipation is not included.

The results without the correction factor of 1.7 are also included in Fig. 2 as dashed lines. It is clearly observed that the drag coefficients taken directly from Sánchez-González et al. (2011) are too small for the present theory, where the reduction of the in-canopy velocity is a part of the solution.

3. Common parameters in the numerical examples

Throughout the remainder of this work, $c_{Dx} = 1.0$ will be used for simplicity in the numerical results together with $c_{mx} = c_{mz} = c_{Dz} = 0$. Furthermore, the rigid vegetation has a uniform cross section over its length, and the cross section is assumed circular with a diameter of $d = 0.01$ m. The number of stems are fixed to 0, 300, 900 and 1500. This equals to porosities of 1.000, 0.929, 0.976 and 0.882, respectively.

The use of a constant drag coefficient irrespectively of the wave height and period does not match the dependency of the KC-number as found by e.g. Sánchez-González et al. (2011), but the results will still show the correct qualitative behaviour.

4. Vertical variation of pressure and velocities

The vertical variation of the primitive variables u, w and p are briefly described in this section through a plot of the magnitude of these variables: U, W and P. The velocities are made non-dimensional with the velocities based on non-dissipative linear wave theory:

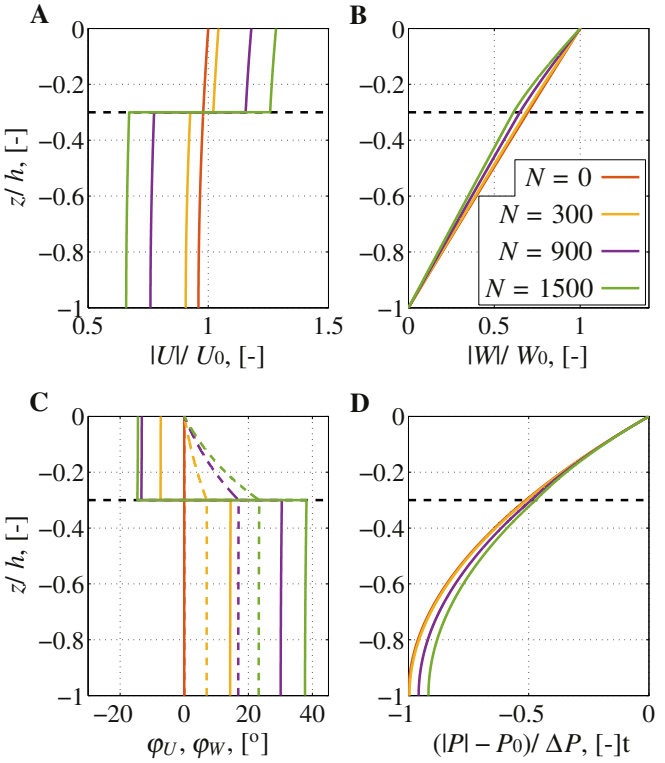

Fig. 3. Variation in the primitive variables as a function of the number of stems, N. $h = 1$ m, $H = 0.2$ m, $\alpha = 0.3$, $T = 7$ s. All variables are depicted for $x = 0$. A: The absolute value of the nondimensional horizontal velocity. B: The absolute value of the nondimensional vertical velocity. C: The phase lags of the horizontal velocity with the free surface (full line) and the vertical velocity with the free surface (dashed line). D: The nondimensional pressure.

$$U_0 = \frac{\pi H}{T}\frac{\cosh k_{\alpha=1}h}{\sinh k_{\alpha=1}h}$$
$$W_0 = \frac{H}{2}\sigma \tag{36}$$

Here, $k_{\alpha=1}$ is the solution to the linear dispersion relation. The non-dimensional pressure is given as $(|P| - P_0)/\Delta P$, where P_0 and ΔP are given as

$$P_0 = \rho g\frac{H}{2} \quad \text{and} \quad \Delta P = P0 - \rho g\frac{H}{2}\frac{1}{\cosh k_{\alpha=1}h} \tag{37}$$

The phase lag between the velocity coefficients U and W and the free surface is also depicted in Fig. 3, where the phase lags are defined as follows:

$$\varphi_U = \arctan\frac{\mathrm{Im}[U]}{\mathrm{Re}[U]} \quad \text{and} \quad \varphi_W = \arctan\frac{\mathrm{Im}[W]}{\mathrm{Re}[W]} - \frac{\pi}{2} \tag{38}$$

Note that the phase lags of P relative to the free surface was also computed, but not depicted, since it was less than 1°.

The variation of the (filter) velocities are in line with the expectations, namely that there is a reduction of the horizontal (filter) velocity inside of the canopy. The increase in the horizontal velocity above the canopy follows from the shortening of the waves with increasing density of the canopy. The vertical velocity simply decreases from the free surface to vanish at the bottom.

The pressure inside of the canopy increases with an increase of the density of the canopy. This is explained by Eq. (15) and this increase in pressure with increase in flow resistance can (partly) explain the relative smaller reduction in the horizontal velocity inside the canopy in the case of waves in comparison with pure current, see Luhar et al. (2010). The physical explanation is that since the vertical velocity only decreases a little with an increasing density of the canopy, the reduction in the horizontal velocity must be small as well (due to the continuity equation). As a result, the pressure must increase to overcome the additional flow resistance inside of the canopy.

Finally, it is observed that the phase lags (Fig. 3C) are not zero as soon as $N > 0$. $\varphi_W = 0$ at $z = 0$ due to the free surface boundary condition, while φ_U is practically piecewise constant inside and above the vegetation. Since $|\varphi_U - \varphi_W| \neq 90^\circ$ it holds that $\overline{uw} \neq 0$. This term represents a shear stress due to the organised orbital motion. This term was already analysed previously for dissipation of wave energy in boundary layers and due to wave breaking (Deigaard and Fredsøe, 1989) and in the context of wave dissipation over canopies in Luhar et al. (2010). This term will contribute to the vertical shear stress distribution over the entire water column and it is currently being analysed by the author.

5. Wave energy density and wave energy flux

Large scale spectral wave models like SWAN and XBeach solve for the transformation of spectral wave energy under the influence of sources and sinks such as wind, bottom friction, wave breaking and vegetation (Suzuki et al., 2011; Van Rooijen et al., 2016). The spatial change in the wave energy density – an transport equation for wave action – relies on the relation

$$E_f = c_f E \tag{39}$$

where E_f is the wave energy flux, c_f is a transport velocity and E is the energy density in the wave (Holthuijsen, 2007)[1] . The magnitude of c_f is the group velocity from non-dissipative linear wave theory (c_g), which is defined Eq. (1). The validity of having $c_f = c_g$ for dissipative waves propagating over a canopy is analysed in this section. The recent work by Cao et al. (2015), where dissipation due to vegetation is included in the mild slope equations, also rely on the assumption $c_f = c_g$.

The wave energy density is given as (Mei, 1999):

$$\begin{aligned} E =& \overline{\int_{-h}^{\eta} \rho g z \mathrm{d}z} + \frac{\rho}{2n} \overline{\int_{-h}^{-\alpha h} \mathrm{Re}[u]^2 + \mathrm{Re}[w]^2 \mathrm{d}z} \\ &+ \frac{\rho}{2} \overline{\int_{-\alpha h}^{\eta} \mathrm{Re}[u]^2 + \mathrm{Re}[w]^2 \mathrm{d}z} \\ =& E_p + E_{k,-} + E_{k,+} \end{aligned} \tag{40}$$

Here, E_p is the potential wave energy density, and $E_{k,-}$ and $E_{k,+}$ the kinetic wave energy densities inside and above the canopy. The presence of $1/n$ in the second term is due to the influence of the porosity on the kinetic energy inside the canopy. In this work, only submerged vegetation is considered, thus $0 < \alpha$. Therefore, the potential wave energy takes the classical form (Mei, 1999):

$$E_p = \overline{\int_{-h}^{\eta} \rho g z \mathrm{d}z} = \frac{1}{16} \rho g H^2 e^{2k_i x} \tag{41}$$

[1] The methods actually solve for the transport of the quantity $E\sigma$, but this is of no importance in this context.

The contributions to the kinetic wave energy density is defined as follows to ease the description of the remaining second order quantities:

$$E_k = E_{k,u-} + E_{k,w-} + E_{k,u+} + E_{k,w+} \tag{42}$$

Each of these terms are given as follows:

$$E_{k,u-} = \frac{\rho}{2n} \overline{\int_{-h}^{-\alpha h} \mathrm{Re}[u]^2 \mathrm{d}z} = \rho \frac{DD^*}{4n} \frac{kk^*}{r_x r_x^*} C_{1-} e^{2k_i x} \tag{43}$$

$$E_{k,w-} = \frac{\rho}{2n} \overline{\int_{-h}^{-\alpha h} \mathrm{Re}[w]^2 \mathrm{d}z} = \rho \frac{DD^*}{4n} \frac{\kappa\kappa^*}{r_z r_z^*} C_{2-} e^{2k_i x} \tag{44}$$

$$\begin{aligned} E_{k,u+} &= \frac{\rho}{2} \overline{\int_{-\alpha h}^{\eta} \mathrm{Re}[u]^2 \mathrm{d}z} \simeq \frac{\rho}{2} \overline{\int_{-\alpha h}^{0} \mathrm{Re}[u]^2 \mathrm{d}z} \\ &= \rho \frac{kk^*}{4} \left(AA^* C_{1+} + BB^* C_{2+} + AB^* C_{3+} + A^* B C_{3+}^* \right) e^{2k_i x} \end{aligned} \tag{45}$$

$$\begin{aligned} E_{k,w+} &= \frac{\rho}{2} \overline{\int_{-\alpha h}^{\eta} \mathrm{Re}[w]^2 \mathrm{d}z} \simeq \frac{\rho}{2} \overline{\int_{-\alpha h}^{0} \mathrm{Re}[w]^2 \mathrm{d}z} \\ &= \rho \frac{kk^*}{4} \left(AA^* C_{2+} + BB^* C_{1+} + A^* B C_{3+} + AB^* C_{3+}^* \right) e^{2k_i x} \end{aligned} \tag{46}$$

The wave induced energy flux to second order is given as (Mei, 1999):

$$E_f = \int_{-h}^{0} \mathrm{Re}[p] \mathrm{Re}[u] \mathrm{d}z \tag{47}$$

In this case, the effect of the porosity cancels out and the energy flux integrated over the entire water column is found as:

$$E_f = \frac{2}{kk^*} \left(\sigma k_r E_{k,u+} - n \mathrm{Im}\left[k r_x^*\right] E_{k,u-} \right) \tag{48}$$

In the limit of no vegetation and deep water it follows that

$$E_f = 2 \frac{\sigma}{k_r} E_{k,u+} = \frac{1}{2} cE = c_g E \tag{49}$$

since $4E_{k,u+} = E$ in deep water and $c = \sigma/k_r$ is the propagation speed. It also holds that $c_g = c/2$ in deep water. Thus the present theory conforms with linear (non-dissipative) wave theory as exemplified by a comparison with deep water wave theory.

In this work, the vegetated group velocity of the wave energy density will be given based on its dynamic definition (Mei, 1999):

$$c_f = \frac{E_f}{E} \tag{50}$$

The kinematic definition of the group velocity (Mei, 1999)

$$c_\delta = \frac{\partial \sigma}{\partial k} \tag{51}$$

will also be addressed. An analytical solution for c_δ based on the extended dispersion relation in Eq. (19) has not been found, because the resistance coefficients r_x, r_z, κ and the closure in Eq. (21) all depend on σ. As a result hereof, it has not been possible to isolate σ. The derivative $\partial\sigma/\partial k$ was evaluated numerically. Note that $c_f = c_\delta = c_g$ in the limit of non-dissipative waves, i.e. $k_i = 0$.

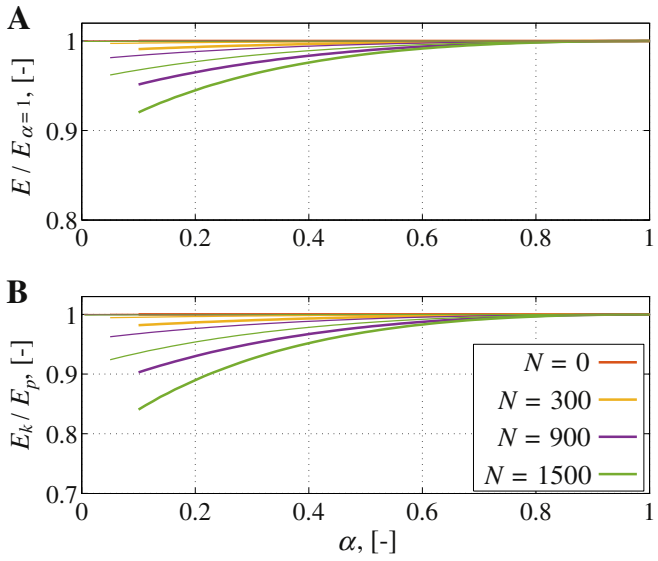

Fig. 4. A: The variation in the total, normalised wave energy density as a function of α and N. B: The ratio between the kinetic and potential energy as a function of α and N. Increasing line thickness refers to an increasing wave height. Thin: $H = 0.01$ m. Medium: $H = 0.10$ m. Thick: $H = 0.20$ m. $h = 1.0$ m and $T = 4.0$ s.

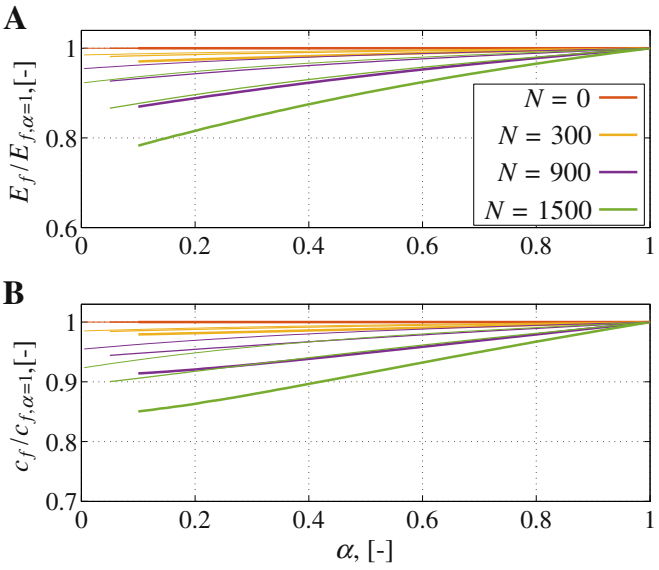

Fig. 5. A: The variation in the total, normalised wave energy flux as a function of α and N. B: The variation in the vegetated group velocity, c_f, as a function of α and N. The vegetated group velocity is defined in Eq. (50). Increasing line thickness refers to increasing wave height. Thin: $H = 0.01$ m. Medium: $H = 0.10$ m. Thick: $H = 0.20$ m. $h = 1.0$ m and $T = 4.0$ s.

An alternative expression for c_f can be obtained by analysing the partial differential equation for the transport of the wave energy density:

$$\frac{\partial E_f}{\partial x} = \frac{\partial c_f E}{\partial x} = -2nf_x E_{k,u-} \tag{52}$$

The dissipation term on the right-hand side was obtained by inserting the solution to the wave problem into the linearised part of Eq. (21) and keeping $f_z = c_{Dz} = 0$. Assuming that c_f is locally constant, the following expression is obtained:

$$c_f = -\frac{nf_x E_{k,u-}}{k_i E} \tag{53}$$

The numerical values for the two expressions of c_f (Eqs. (50) and (53)) were found to be identical. Consequently, the wave energy flux can also be written as

$$E_f = -\frac{nf_x}{k_i} E_{k,u-} \tag{54}$$

(under the assumption that $f_z = 0$.) This expression can only be evaluated as long as $k_i < 0$, i.e. in the presence of vegetation. It will, however, be seen in the following that E_f has the finite limit from classical non-dissipative linear wave theory as $k_i \to 0$.

5.1. Results

The variation in $E/E_{\alpha=1}$ and E_k/E_p as a function of α, N and H is depicted in Fig. 4. It is first of all seen that the wave energy density decreases with higher vegetation (decreasing α) for a fixed value of H. Since the potential energy (see Eq. (41)) is constant, it means that the kinetic energy decreases with higher vegetation; this is seen from Fig. 4B, where the ratio between E_k and E_p is depicted.

Furthermore, the effect of the number of stems is also included in Fig. 4. It is seen that the more dense the canopy, the larger the difference between E_p and E_k. This is in contrast to the solution in the absence of vegetation, where these two energies are identical; a property that is retrieved for $\alpha = 1$. It was noted in Philips (1980) that the equality $E_p = E_k$ holds for "*any conservative dynamical system undergoing small oscillations*". In the present case, however, the system is neither conservative nor undergoing small oscillations. The latter due to the nonlinear closure term; see Section 2.3.

The variation in the energy flux, $E_f/E_{f,\alpha=1}$, and the vegetated group velocity, $c_f/c_{f,\alpha=1}$ are depicted in Fig. 5 as a function of H, N and α. It is observed that the energy flux decreases for an increasing height of the vegetation; the quantity $c_{f,\alpha=1}$ is the same for all values of N and H. This means that α, N and H all have an effect on the energy flux.

The variation of c_f as a function of the wave period is depicted in Fig. 6. Largely the same behaviour as observed in Fig. 5B is found here, but there are additional observations. For the short wave periods of 1.0 s and 2.0 s, there are local maxima in c_f, which are larger than

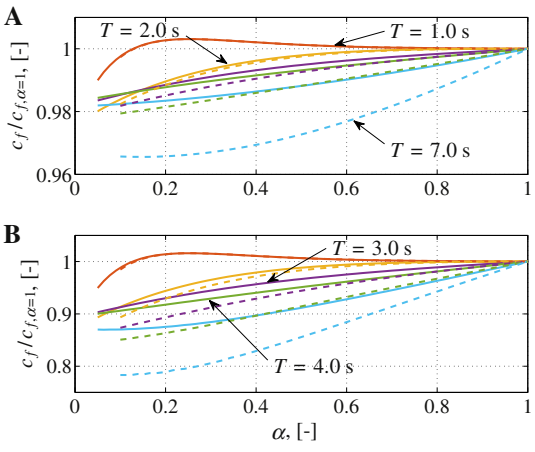

Fig. 6. The relative vegetated group velocity ($c_f/c_{f,\alpha=1}$) as a function of the wave period, wave height, vegetation height and vegetation density. The arrows point to the colour of a given wave period. $h = 1.0$ m. Full line: $H = 0.1$ m. Dashed line: $H = 0.2$ m. A: $N = 300$ stems/m^2. B: $N = 1500$ stems/m^2.

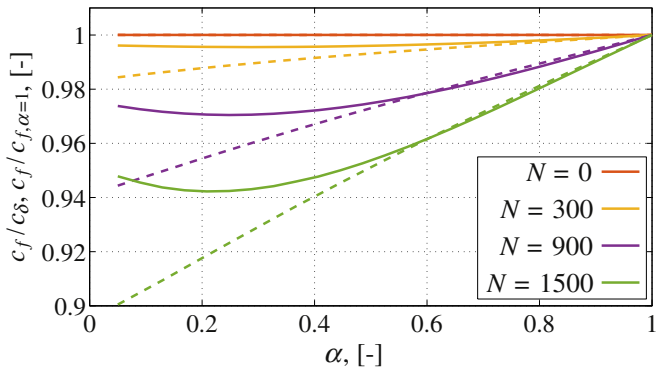

Fig. 7. The difference between the velocities c_δ and c_f. Full line: c_f/c_δ. Dashed: $c_f/c_{f,\alpha=1}$. $h = 1.0$ m, $H = 0.1$ m and $T = 4.0$ s.

the vegetated group velocity for no vegetation. This behaviour is ascribed to the fact that the waves are in, or close to, deep water conditions for $T = 1.0$ s and $T = 2.0$ s when $\alpha = 1$. An increase in the vegetation height is qualitatively identical to a decrease in the water depth, which leads to shorter waves; see discussion regarding the term "effective water depth" in Losada et al. (1997). It is well known from classical linear wave theory that the group velocity has a local maximum between deep and shallow water and this similar effect is observed here with a change in the properties of the canopy. A decrease of almost 15% is seen in c_f relative to $\alpha = 1$ is observed for $h = 1.0$ m and $H = 0.1$ m in the shallow water limit; a discrepancy that increases with an increasing wave height.

A comparison between the two definitions of the group velocity, see Eqs. (50) and (51), is presented in Fig. 7 for $T = 4$ s and $H = 0.1$ m in a water depth of $h = 1.0$ s. It is clearly seen that $c_f \neq c_\delta$. Consequently, the wave energy density is not transported by the group velocity as defined by the differentiation $\partial\sigma/\partial k$. In the case of $N = 0$ the solution $c_f = c_g = c_\delta$ is retrieved.

The dashed lines in Fig. 7 depicts the ratio $c_f/c_{f,\alpha=1}$, thus it is seen that the c_δ is practically equal to the group velocity as evaluated by Eq. (1) up to a certain height of the vegetation; in this case $\alpha = 0.6$.

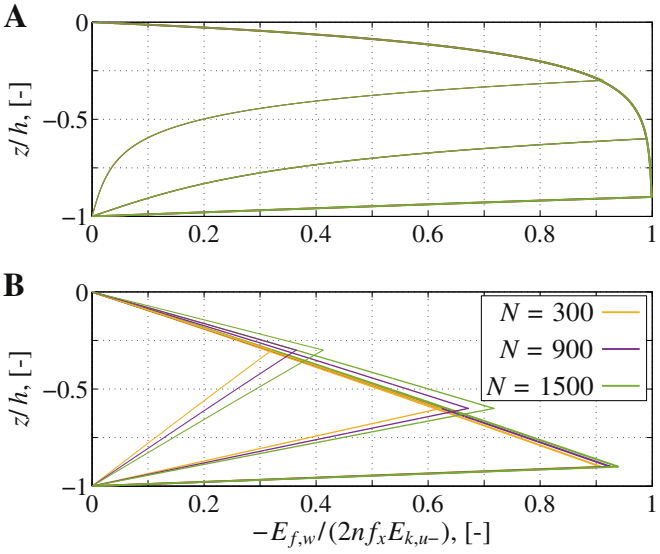

Fig. 8. The vertical variation in the vertical wave energy flux as a function of α and N. Thin line: $\alpha = 0.3$. Medium line: $\alpha = 0.6$. Thick line: $\alpha = 0.9$. In all cases, $H = 0.1$ m and $h = 1.0$ m as in Fig. 3. A: $T = 1.0$ s. B: $T = 7.0$ s.

The vertical wave energy flux at any given level z is expressed as

$$E_{f,w} = \overline{\mathrm{Re}[p]\mathrm{Re}[w]} = \frac{1}{4}\left(PW^* + P^*W\right) \tag{55}$$

This quantity is plotted in nondimensional form in Fig. 8, where $E_{f,w}$ is made nondimensional with the total energy dissipation $2nf_xE_{k,u-}$. Fig. 8 shows that the energy is extracted from the entire water column and dissipated inside the canopy (the kinks in $E_{f,w}$ indicates the top of the canopy). The larger the value of α, the larger the ratio of the dissipated energy that originates from above the canopy, while the remaining dissipated wave energy originates from inside the canopy itself. It is also worthwhile to notice that while the values of $-E_{f,w}/(2nf_xE_{k,u-})$ are almost constant for 300 to 1500 stems/m^2, the values of $E_{f,w}$ varies by a factor of 2.5–4.0 between $N = 300$ and $N = 1500$.

The results concerning the vertical wave energy flux are similar to the results by Deigaard and Fredsøe (1989), who found that the wave energy extracted in wave boundary layers originate from the entire water column. They found a triangular distribution of $E_{f,w}$ that vanished at the still water level; this shape was found, because Deigaard and Fredsøe (1989) limited the analysis to shallow water wave theory.

The present results describing an extraction of wave energy from all over the water column are similar to the those of Deigaard and Fredsøe (1989). Here, it was shown that the wave energy dissipated in a wave boundary layer originated from the whole of the water column.

The vertical energy flux is finite because p and w are *not* out of phase in dissipative waves. In the case of no vegetation (and omission of dissipation in the wave boundary layer, Deigaard and Fredsøe, 1989), $E_{f,w} = 0$ is retrieved.

6. Radiation stress tensor

The radiation stress tensor in the presence of vegetation was already derived in Mendez et al. (1998), but it is included in this work for consistency. No results will be presented.

Following Longuet-Higgins and Stewart (1964), the mean pressure below the trough level deviates from the hydrostatic pressure, because of the organised vertical transport of vertical momentum. Modifying the approach by Longuet-Higgins and Stewart (1964) to account for the effect of porosity, the radiation stress component in the direction of propagation, S_{xx}, is given as:

$$S_{xx} = E_p + 2\left[E_{k,u-} + E_{k,u+} - E_{k,w-} - E_{k,w+}\right] \tag{56}$$

The transverse component does not include the effect of the horizontal velocity component, so it reads:

$$S_{yy} = E_p - 2\left[E_{k,w-} + E_{k,w+}\right] \tag{57}$$

where y is the horizontal coordinate perpendicular to the direction of wave propagation. In the present case, where the orbital velocity along y is 0, the cross component of the radiation stress tensor vanishes.

The gradients in the radiation stress tensor along the direction of wave propagation are:

$$\frac{\partial S_{xx}}{\partial x} = 2k_iS_{xx} \quad \text{and} \quad \frac{\partial S_{yy}}{\partial x} = 2k_iS_{yy} \tag{58}$$

Since $\partial S_{xx}/\partial x$ does not vanish, when $k_i < 0$, there will be a mean setup of the water surface to balance this force. This was already studied in Mendez et al. (1998) and Dean and Bender (2006), though

only Dean and Bender (2006) included the important term of the mean force from the vegetation acting on the water column. This contribution results in a reduction in the wave induced setup, which has been studied both experimentally (Wu et al., 2011) and numerically (Van Rooijen et al., 2016).

7. Stokes drift

The Stokes drift is the additional mass flux due to the presence of waves. The open orbital motion of the water particles is a consequence of the Stokes drift, see e.g. Van Dyke (2005) for a visualisation. In the following, both the vertical distribution of the drift velocity and the resulting volume flux will be derived.

There are two classical approaches to obtain the magnitude of the mass flux: the Eulerian and the Lagrangian approaches. While the vertical distributions of the drift velocities differ between the two approaches, the vertically integrated volume flux is identical in the case of no vegetation ($\alpha = 1$), see e.g. Fredsøe and Deigaard (1992).

The effect of submerged vegetation on the Stokes drift velocity and volume flux will be analysed in this section. Both the Eulerian and Lagrangian approaches will be described. It will also be addressed, whether the resulting expressions for the volume flux are identical through two approaches to evaluate the vertical, Lagrangian Stokes velocity at $z = 0$.

7.1. Eulerian Stokes drift

The Eulerian Stokes drift is derived based on the integral of the horizontal velocities between the trough level and the instantaneous surface elevation, η (see e.g. Fredsøe and Deigaard, 1992). The vertical distribution of the Eulerian drift velocity is given as

$$\begin{aligned}\bar{u}_E &= \frac{1}{T}\int_{-\lambda}^{+\lambda} \mathrm{Re}[U_+|_{x=0,\ z=0}]\cos(\sigma t - k_r x)e^{k_i x}\mathrm{d}t \\ &= \frac{\mathrm{Re}[U_+|_{x=0,\ z=0}]e^{k_i x}}{\pi}\sqrt{1-\left(\frac{2z}{He^{k_i x}}\right)^2}\end{aligned} \tag{59}$$

Here, $\lambda = \sigma^{-1}\arccos(2z/(H\exp k_i x))$. Only the real part of U_+ contributes to $\bar{u}_E$, because the imaginary part is multiplied by $\sin(\sigma t - k_r x)$, which is out of phase with η. The expression in Eq. (59) is valid in the interval $-H/2\exp k_i x \le z \le H/2\exp k_i x$.

The vertical integration of $\bar{u}_E$ yields the Eulerian volume flux:

$$q_E = \int_{-H/2\exp k_i x}^{H/2\exp k_i x} \bar{u}_E \mathrm{d}z = \frac{H}{4}\mathrm{Re}[U_+|_{x=0,\ z=0}]e^{2k_i x} \tag{60}$$

The expressions in Eqs. (59) and (60) are practically identical with those for waves propagating over a non-vegetated water column. The Eulerian Stokes drift was already formulated by Mendez et al. (1998) for a vegetated water column, though they did not discuss the magnitude as a function of e.g. properties of the canopy.

7.2. Lagrangian Stokes drift

The Lagrangian Stokes drift is obtained by following the water particles along their trajectories. A Taylor expansion of the trajectory around a mid-point yields the following approximation of the Lagrangian motion given in terms of Eulerian quantities (Philips, 1980):

$$\begin{aligned}\bar{u}_L =& \frac{\partial}{\partial x}\mathrm{Re}[Ue^{i\theta}]\bar{\int}\mathrm{Re}[Ue^{i\theta}]\mathrm{d}t \\ &+ \frac{\partial}{\partial z}\mathrm{Re}[Ue^{i\theta}]\bar{\int}\mathrm{Re}[We^{i\theta}]\mathrm{d}t\end{aligned} \tag{61}$$

Philips (1980) furthermore notes that $\bar{w}_L = 0$ over the entire water column for linear (non-dissipative) wave theory in an arbitrary water depth. This property will be evaluated for the vegetated case in Section 7.3.

The evaluation of Eq. (61) is trivial, but tedious, to derive, so the expressions are merely stated here:

$$\bar{u}_{L,+} = \frac{1}{2c}\left[U_+U_+^* + W_+W_+^*\right]e^{2k_i x} \quad \text{for } -\alpha h < z \le 0 \tag{62}$$

above the canopy. $c = \sigma/k_r$. Inside the canopy the Stokes drift velocity is given as:

$$\bar{u}_{L,-} = \frac{1}{n}\left[\frac{1}{2c}U_-U_-^* + \frac{1}{2\sigma}\mathrm{Re}\left[\frac{kr_z}{r_x}\right]W_-W_-^*\right]e^{2k_i x} \tag{63}$$

This holds for $h \le z < -\alpha h$. The expressions are conceptually identical with the expressions for the non-vegetated case (see e.g. Mei, 1999).

Integration over the vertical yields the volume flux contributions. Above the canopy this reads

$$q_{L,+} = \int_{-\alpha h}^{0}\bar{u}_{L,+}\mathrm{d}z = \frac{1}{\rho}\frac{2}{c}\left(E_{k,u+} + E_{k,w+}\right) \tag{64}$$

Inside the canopy the volume flux is given as:

$$q_{L,-} = \int_{-h}^{-\alpha h}\bar{u}_{L,-}\mathrm{d}z = \frac{1}{\rho}\left(\frac{2}{c}E_{k,u-} + \frac{2}{\sigma}\mathrm{Re}\left[\frac{kr_z}{r_x}\right]E_{k,w-}\right) \tag{65}$$

The drift velocity at the interface, $\bar{u}_{L,\alpha}$, is undefined, because of the discontinuity in the horizontal velocity at the top of the canopy, see Fig. 3. The volume flux, however, can still be derived. First, the horizontal pore velocities adjacent to the top of the canopy are approximated by a step function:

$$\begin{aligned}u_\alpha &= U_\alpha e^{i\theta} \\ &= e^{i\theta}\times\begin{cases} k/\sigma\cosh\kappa h(1-\alpha)D & ,\ z = -\alpha h - \epsilon \\ ik/(nr_x)\cosh\kappa h(1-\alpha)D & ,\ z = -\alpha h + \epsilon\end{cases}\end{aligned} \tag{66}$$

where ϵ is an infinitesimal, positive value. Consequently, the vertical gradient of u_α in terms of pore velocities can be defined as:

$$\frac{\partial}{\partial z}U_\alpha e^{-i\theta} = k\left(\frac{1}{\sigma} - \frac{i}{nr_x}\right)\cosh\kappa h(1-\alpha)De^{i\theta}\delta(z+\alpha h) \tag{67}$$

$$= \Delta U_\alpha e^{i\theta}\delta(z+\alpha h) \tag{68}$$

Here, $\delta(z+\alpha h)$ is the Dirac delta function, i.e. the gradient is essentially unknown, but the flux can still be defined as:

$$\begin{aligned}q_{L,\alpha} &= \int_{-\alpha h-\epsilon}^{-\alpha h+\epsilon}\overline{\frac{\partial}{\partial z}\mathrm{Re}\left[U_\alpha e^{i\theta}\right]\int\mathrm{Re}\left[W_\alpha e^{i\theta}\right]\mathrm{d}t}\mathrm{d}z \\ &= \frac{i}{4\sigma}\left(\Delta U_\alpha W_\alpha^* - \Delta U_\alpha^* W_\alpha\right)\end{aligned} \tag{69}$$

where $W_\alpha = -\kappa/r_z\sinh\kappa h(1-\alpha)D$ is the vertical filter velocity at $z = -\alpha h$. It is not necessary to distinguish between filter and pore velocities for the vertical velocity, because the correction with porosity drops out during the integration over the vertical. If the correction for porosity was included, the integral in Eq. (69) should have been divided into two parts: above and below the interface $z = -\alpha h$.

Finally, the total Lagrangian mass flux is given as follows:

$$q_L = q_{L,-} + q_{L,\alpha} + q_{L,+} \tag{70}$$

At this point, it is difficult to judge, whether q_E and q_L are identical, due to the complexity of q_L. This equality will be analysed in the following section.

7.3. Vertical Lagrangian Stokes velocity

The vertical component of the Stokes drift at the free surface ($z = 0$) will be analysed in this section. Following Philips (1980), this reads:

$$\bar{w}_L|_{z=0} = \frac{\partial}{\partial x}\mathrm{Re}[W_+ e^{i\theta}]\int \mathrm{Re}[U_+ e^{i\theta}]\mathrm{d}t\,|_{z=0} + \frac{\partial}{\partial z}\mathrm{Re}[W_+ e^{i\theta}]\int \mathrm{Re}[W_+ e^{i\theta}]\mathrm{d}t\,|_{z=0} \quad (71)$$

Philips (1980) furthermore states that $\bar{w}_L|_{z=0} = 0$ for non-dissipative waves propagating over a horizontal bed.

Utilising that the vertical velocity at the free surface is identical to $\partial\eta/\partial t$, it is straightforward to evaluate Eq. (71). The result reads:

$$\bar{w}_L|_{z=0} = -2k_i\frac{H}{4}\mathrm{Re}\left[U_+|_{x=0,z=0}\right]e^{2k_i x} = -2k_i q_E \quad (72)$$

Since the Eulerian velocity field fulfills the continuity equation, the Lagrangian velocity field has to fulfill the continuity equation on its own. The continuity equation for the Lagrangian velocity field reads:

$$\frac{\partial \bar{u}_L}{\partial x} + \frac{\partial \bar{w}_L}{\partial z} = 0 \quad (73)$$

Solving for $\bar{w}_L|_{z=0}$ leads to the following expression:

$$\bar{w}_L|_{z=0} = -\int_{-h}^{\eta}\frac{\partial \bar{u}_L}{\partial x}\mathrm{d}z \simeq -2k_i\int_{-h}^{0}\bar{u}_L\mathrm{d}z = -2k_i q_L \quad (74)$$

Both Eqs. (71) and (73) are based on a Lagrangian framework, so the two expressions for $\bar{w}_L|_{z=0}$ must necessarily be identical. As a consequence hereof, the above analysis has shown that $q_E \equiv q_L$, even though it is hard to discern from the mathematical expression of q_L and q_E.

The vertical distribution of $\bar{w}_L$ can be deduced from Eq. (74). $\bar{w}_L$ will be 0 at the bottom and increase in a monotone fashion to $z = -\alpha h$, where a discontinuity is present due to $q_{L,\alpha}$. Hereafter, $\bar{w}_L$ will again increase in a continuous and monotone fashion up to $z = 0$.

The fact that the drift velocity is finite at the surface suggests that the volume of water needed for the initial build-up of the wave-induced setup is (at least partly) obtained from the horizontal gradient in the Stokes drift. This also means that the present work only represents the initial stage of the interaction between waves and vegetation, since additional processes are required to prevent the water level from rising indefinitely. This will be discussed further below.

7.4. Results

The vertical distribution of the horizontal Lagrangian Stokes velocity, $\bar{u}_L$, is depicted in Fig. 9 for various values of the vegetation density and the wave period. The normalisation used in Fig. 9 is the same as utilised in Fredsøe and Deigaard (1992). It is observed that the discontinuity between the upper and lower part of the water column increases with the period. This is caused by the increase in the orbital velocities at $z = -\alpha h$ for an increasing wave period (going from deep to shallow water conditions with an increase in the wave period). The magnitude of the Stokes drift (q_E or q_L) and the volume flux $q_{L,\alpha}$ are tabulated in Table 1 for the conditions in Fig. 9.

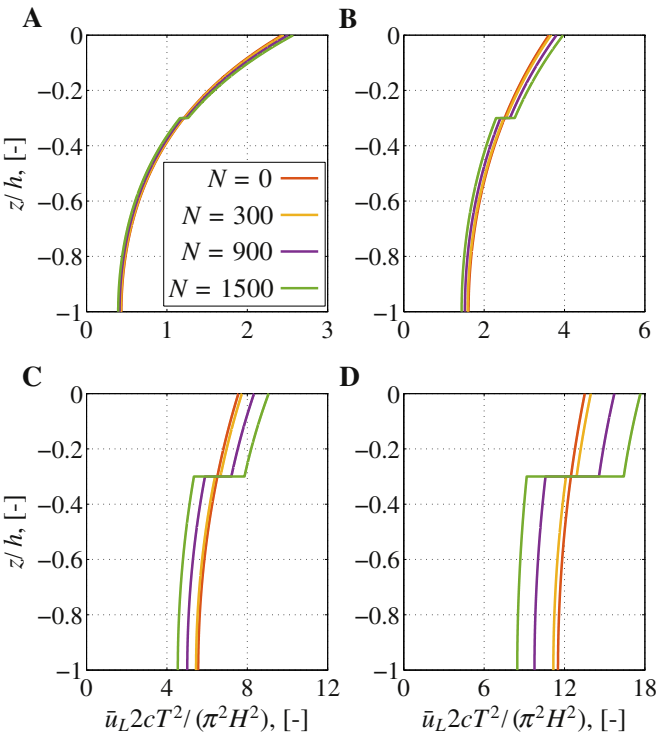

Fig. 9. The distribution of the Lagrangian Stokes drift velocity, $\bar{u}_L$, for $h = 1.0$ m, $\alpha = 0.3$ and $H = 0.1$ m. Four vegetation densities are depicted in each panel. A: $T = 2$ s. B: $T = 3$ s. C: $T = 5$ s. D: $T = 7$ s. For all panels, the Lagrangian velocity at $z = -\alpha h$ is undefined.

The total Stokes drift (Lagrangian and Eulerian) is affected by the vegetation in such a way that the Stokes drift increases with increasing vegetation height (decreasing α) and decreasing $k_{\alpha=1}h$ (increasing wave period), see Fig. 10. This effect is more pronounced in shallow waters. It is seen that q_E becomes almost 15% larger for given wave parameters (shallow water), when the non-vegetated and the vegetated results were compared.

The resulting distribution of the Lagrangian drift velocities is also depicted in Fig. 10. The ratios $q_{L,+}/q_E$, $q_{L,-}/q_E$ and $q_{L,\alpha}/q_E$ are depicted. The most remarkable observation is that the Stokes drift at the interface can become as large as 10–20% of the total Stokes drift in the shallow water limit. Again, this is most pronounced in shallow waters. Nonetheless, this additional advection mechanism can have an effect on the advection of both sediment and biological matter; e.g. spores from the vegetation itself.

The value of $\bar{w}_L|_{z=0}$ attained was as large as 3.5 mm/s for the cases depicted in Fig. 10. A simple test with a wave height of $H = 0.20$ m gave a maximum value of 13.0 mm/s, which indicates that $\bar{w}_L|_{z=0}$ scales approximately with H^2. The remaining contributions: q_E, $q_{L,+}$, $q_{L,\alpha}$ and $q_{L,-}$ also scale with H^2.

Table 1
The total volume flux due to the Stokes drift (q_E or q_L) and the Lagrangian volume flux at the interface ($q_{L,\alpha}$). The values corresponds to the conditions depicted in Fig. 9.

	$N = 0$		$N = 300$		$N = 900$		$N = 1500$	
T	q_E	$q_{L,\alpha}$	q_E	$q_{L,\alpha}$	q_E	$q_{L,\alpha}$	q_E	$q_{L,\alpha}$
s	$10^3 \cdot$ m^3/m/s		$10^3 \cdot$ m^3/m/s		$10^3 \cdot$ m^3/m/s		$10^3 \cdot$ m^3/m/s	
2.0	18.8	0.00	19.0	0.03	19.4	0.18	19.9	0.38
3.0	16.9	0.00	17.1	0.09	17.8	0.55	18.6	0.99
5.0	16.1	0.00	16.4	0.28	17.7	1.32	18.9	1.94
7.0	15.9	0.00	16.4	0.53	18.2	1.92	19.7	2.48

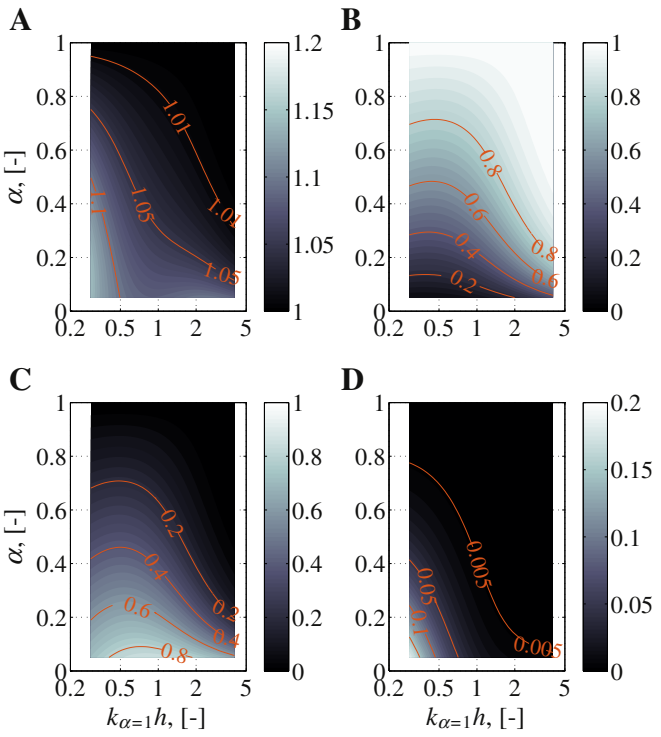

Fig. 10. A: $q_E/q_{E,\alpha=1}$ s. B: $q_{L,+}/q_E$ s. C: $q_{L,-}/q_E$. D: $q_{L\alpha}/q_E$. For all panels: $h = 1.0$ m, $H = 0.1$ m and $N = 1500$ stems/m^2. The period range from 1.0–7.0 s.

In the case of a closed flume, the return flow must balance the Stokes drift in the steady-state situation, i.e. the gradient in the volume flux due to the return flow must equal $\bar{w}_L|_{z=0}$. The same must hold for the steady-state solution for any wave–current interaction over a canopy.

8. Discussion

8.1. Re-visiting the assumptions

A few of the assumptions will be further discussed in this section: no wave breaking, no reflection from the shoreward end of the canopy and rigid stems. The omission of wave breaking is not considered to be a major problem, since the experimental data from Wu et al. (2011) clearly showed that the dissipation due to vegetation is more prominent than wave breaking (the waves never became steep enough inside the canopies). Wave breaking, however, can still offer a considerable mechanical wear at the edge of the canopy.

The presence of reflection from the shoreward end of the canopy was treated by Méndez et al. (1999), who considered the effect on the surface elevation inside of the canopy. The forward propagating wave has a wave height of H as $x = 0$, which is a distance of λ from the shoreward end of the canopy. Assume that the reflection coefficient $R = \mathcal{O}(0.1)$. The reflected wave height at $x = 0$ is then

$$H_R = RHe^{2k_i\lambda} \tag{75}$$

The influence of a reflected wave field on the radiation stress tensor was previously derived in Jacobsen et al. (2015) in the context of internal setup inside of a permeable revetment. They found that the radiation stress tensor has an additional contribution from the reflected wave ($R^2e^{4k_i\lambda}H^2$), but also a cross-term from the combined forward propagating and reflected waves ($Re^{2k_i\lambda}H^2$). This cross-term does not vanish, because u^2 is without directionality. This means that a reflected wave will introduce a correction to the second-order terms (energy density and radiation stress tensor). The magnitude of this correction will depend on λ and the resistance properties of the canopy. The closer to the shoreward end, the larger the effect. The resistance properties (N, d and α), on the other hand, will give rise to a larger reflection for more dense canopies, but denser canopies suggests an increase in $|k_i|$, thus effectively reducing the effect of reflected waves well inside the canopy with respect to the second order terms. Consequently, assuming that $R = \mathcal{O}(0.1)$, the correction factor will be even smaller.

Because of the directionality of the Stokes drift, it is easy to show that the cross-term disappears, thus the Stokes drift will be corrected by a factor $(1 - R^2e^{4k_i\lambda})$, i.e. merely a few percentages.

Submerged, rigid vegetation is not often encountered in nature (mangroves are typically emerged), however, the present theory can also be used for submerged reefs or breakwaters. When it comes to vegetation, then some laboratory data suggests the rigidity cannot be defined in an absolute sense. The derivation of the concept of effective length in Luhar and Nepf (2016) showed that even (weakly) flexible stems were subject to identical forces and thus likely dissipated an equal amount of wave energy. Consequently, rigidity could be relaxed to a definition, where the vegetation is rigid enough to dissipate an comparable amount of wave energy as fully rigid stems. Due to the complexity and nonlinearity of motion of vegetation (Dijkstra and Uittenbogaard, 2010), an analytical model capable of for instance addressing the energy flux inside of a canopy with nonlinear deformation seems out of reach.

8.2. Shoaling and refraction

The results in relation to the vegetated group velocity (see Fig. 5) and the non-equal splitting between E_k and E_p (see Fig. 4) lead to some qualitative observations on the behaviour of a wave as it propagates through a canopy.

First of all, the dominating feature in the canopy is the dissipation of the wave energy. This means that for given canopy properties, the vegetated group velocity will increase as H decreases; see Fig. 5. This change in vegetated group velocity is similar to shoaling to a larger water depth, i.e. the wave height decreases not only due to the dissipation but also due to shoaling effects. This additional decay in the wave height is further enhanced through the increase in E_k/E_p as H decreases; see Fig. 4. Consequently, the smaller the wave height the closer E_k/E_p is to 1, so energy must be transferred from E_p to E_k as the dissipation takes place; this is an apparent dissipation of wave energy. This shows that a part of the decay in the wave height is conservative: the decay in the wave height is not uniquely attributed to dissipation. The transfer mechanism of the energy density from potential to kinetic has not been identified.

One of the outcomes of this theory is that the wave length becomes smaller with increasing flow resistance (see also Gu and Wang, 1991), i.e. the propagation speed decreases with increasing flow resistance. For a certain canopy, it also means that the waves will propagate gradually faster, as the wave energy dissipates. Consequently, spatial gradients in either the resistance of the canopy or the wave height will lead to curving wave fronts, i.e. refraction. The propagation speed, however, is smaller than outside of the canopy in an equal depth, i.e. it is likely that the wave fronts will bend towards edges of a canopy that are (initially) parallel to the direction of propagation. Therefore, the refraction effect attracts the wave energy into the canopy (see the surface elevation plot in Ma et al., 2013, their figure 13).

On the lee side of the canopy, the wave resumes propagation according to linear wave theory, i.e. $E_k = E_p$ and $c_f = c_g$. This means that a part of E_p will be transferred to E_k and this transfer will be perceived as an additional dissipation across the lee edge of the vegetation. In addition to this, the vegetated group velocity will

further increase and this again causes an additional lowering of the wave height due to a mechanism similar to shoaling into larger water depths. The location of this conservative decrease in the wave height is easiest to evaluate in physical model testing. It should be noted that this effect will be hard to measure, if the reduction in wave height over the canopy is large or there are large reflection from the end of the laboratory flume.

Especially the inverse shoaling effects described in this section can have an effect on the estimated resistance properties of a canopy in laboratory and field experiments, since a decrease in wave height is not uniquely due to dissipation of the energy.

8.3. Implication for practical engineering models

The newly derived expressions for c_f and E have direct implications for practical engineering models, e.g. SWAN (Suzuki et al., 2011), and the recent mild-slope formulation with the inclusion of dissipation due to vegetation (Cao et al., 2015).

First of all, the models rely on an assumption of an equal splitting of the wave energy density into the kinetic and potential parts. It was seen in Section 5 that $E_k \leq E_p$, which means that

$$E = \frac{1}{\beta}\rho g H^2 \leq \frac{1}{8}\rho g H^2 \tag{76}$$

Here, the right hand side is the standard expression from non-dissipative, linear wave theory. The resulting wave height is therefore found as

$$\sqrt{\frac{8E}{\rho g}} \leq H = \sqrt{\frac{\beta E}{\rho g}} \tag{77}$$

The consequence is that the wave height is underestimated, when based on E. Adopting the value of $E_k/E_p = 0.84$ from Fig. 4, the underestimation of H is found to be 5%.

The second consequence is that $c_f(h, \sigma, E, r_x(E), \ldots)$ for a given water depth and vegetation properties. This means that the transport equation for the wave energy density with dissipation due to vegetation should take this form:

$$\frac{\partial c_f(h, \sigma, E, r_x(E), \ldots)E}{\partial x} = \bar{\epsilon}_v(h, \sigma, E, r_x(E), \ldots) \tag{78}$$

Here, $\bar{\epsilon}_v$ is the dissipation due to vegetation. The right-hand side is already treated in SWAN, because most of the source terms are non-linear in the wave energy density (Suzuki et al., 2011). The transport term, however, is problematic, because it requires a re-construction of the linear sets of equations per non-linear iteration. A suggestion to the numerical treatment of this added complexity is beyond the scope of this work.

Many models still do a reasonable job without these effects (e.g. Cao et al., 2015; Van Rooijen et al., 2016) and it is likely to be due to the fact that the above mentioned processes are simply included in the one calibration coefficient for the flow resistance (Mendez and Losada, 2004; Sánchez-González et al., 2011). This could be defendable in practical engineering models, but the effect of the correction to the transport equation (Eq. (78)) requires further investigation. In addition to this, the magnitude of the correction term to amongst others the vegetated group velocity and energy distribution between E_k and E_p for irregular and directional spread waves should be investigated further. The latter since the correction terms could become negligible for a sufficient large number of frequencies and directions (small individual wave amplitudes).

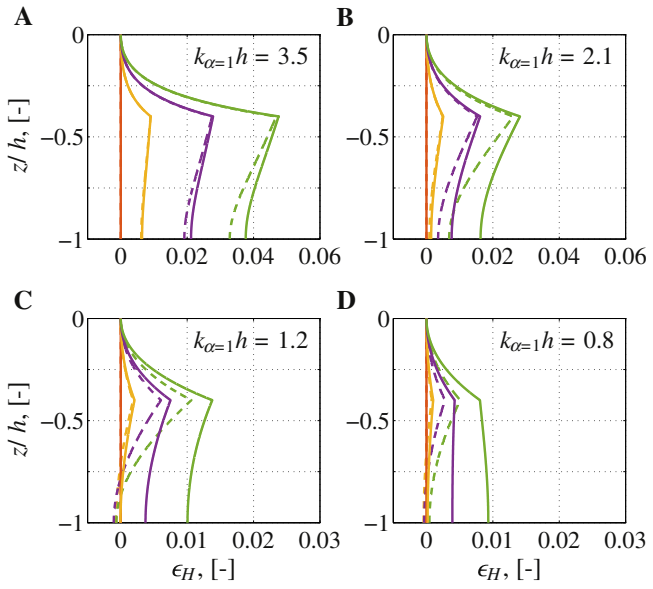

Fig. 11. The discrepancy in the prescribed and reconstructed pressures. Full line: $H = 0.2$ m. Dashed line: $H = 0.1$ m. $T = 2$ s and $\alpha = 0.4$. Colours the same as in Fig. 9.

8.4. Reconstruction of the surface elevation

One way of obtaining the wave height is to measure the pressure signal at a certain distance below the mean surface. The spectrum of the measured pressure can be transferred to the spectrum of the amplitudes based on linear wave theory (see Bishop and Donelan, 1987). While there are instrumental noise in field and laboratory measurements, the current theory allows for a clean evaluation of potential errors due to the presence of vegetation. The error $\epsilon_H = H_r/H - 1$ is discussed in this section, where H_r is the reconstructed wave height.

The error is plotted in Fig. 11 for two wave heights, four densities of the canopy and four water depths. The height of the canopy is constant: $\alpha = 0.4$. The largest discrepancies are for deep water conditions and there is a consistent maximum in the error at the top of the canopy. While the effect of the wave height is small in deep water, the wave height becomes important in intermediate water depths, because the resistance grows with the increasing wave-induced velocities inside the canopy. The resulting errors, however, are small for these water depths.

For short waves (i.e. deep water conditions), it is difficult to reconstruct the wave height, because of instrumental noise (Bishop and Donelan, 1987), consequently, a reconstruction error of some 4% is small in comparison with the potential errors related to the large transfer function and instrumental noise. This suggests that linear wave theory can be applied to reconstruct the surface elevation based on a measured pressure signal inside of a canopy.

These results also suggest that the presence of flexible vegetation will only have a limited effect on the reconstruction of the free surface elevation. The difference between the present theory and the one including flexible vegetation is that the vertical movement of the vegetation will give rise to an additional lowering of the dynamic, wave-induced pressure due to organised motion of the flexible blades (similar to the second order effect on the pressure in the derivation of the radiation stress tensor). The pressure reduction due to organised motion of the blades is likely small in comparison with the reduction due to the orbital motion of the water particles. The effect is not quantified in this work.

Note that the wave height can be estimated using orbital velocities (measured by an ADCP or other current meters). Inspecting the velocity profiles shown in e.g. Fig. 3, it becomes clear that reconstruction of the surface elevation from a velocity profile will introduce much larger errors than the errors originating from a reconstruction based on a pressure signal.

8.5. Order of the solution

The behaviour of $1 - E_k/E_p$ and $1 - c_f/c_{f,\alpha=1}$ has been evaluated as a function of the wave height. It was seen that these quantities behave qualitatively as $\psi \cdot H^{\gamma}$, where $\gamma \in [1.5; 2.0]$ (for the present parameter sets). The periods were chosen between 2.0 s and 10.0 s, the wave heights up to 0.1 m, and the wave depth was 1.0 m. It was found that for the short wave periods, $\gamma = 2.0$, i.e. the correction is a higher order effect, while γ approached 1.5 as the wave periods increased. It was also seen that γ became smaller for an increasing number of stems, where the range 300–1500 was tested. Surprisingly enough, there was only a limited effect of α on γ.

Consequently, the present theory offers correction terms to classical second order wave properties; the magnitude of the correct is somewhere between first and second order in the wave height. The correction to linear wave theory becomes more prominent for longer waves and denser canopies.

9. Conclusion

The present work presents a description of the propagation of waves in the interior of a submerged canopy with anisotropic flow resistance; diffusion was neglected. The theory is based on the assumptions that boundary layer effects on top of the canopy can be neglected, that the waves are (almost) linear and there is no wave breaking. Furthermore, it is assumed that the outer flow is irrotational, while the inner flow is subject to friction.

The second order wave properties such as wave energy density, wave energy flux, the corresponding vegetated group velocity, the radiation stress tensor and the Eulerian and Lagrangian Stokes drifts were derived.

It was shown that the vegetated group velocity does not equal the classical group velocity from non-dissipative linear wave theory and there is an non-equal splitting between the potential, E_p, and kinetic, E_k, wave energy densities. Both of these properties have a direct implication for the large scale modelling of waves in vegetation, since they can cause shoaling, refraction and conservative decay in the wave height due to changes in the ratio E_k/E_p.

The derivations of the Stokes drift have shown that the Eulerian and Lagrangian formulations are identical even in the presence of vegetation, but it is important to include the Lagrangian flux at the top of the canopy due to the discontinuity in the horizontal velocity. The expressions are not easily comparable due to their complexity, but through an evaluation of the finite Stokes velocity at the free surface, it was seen that the horizontal Eulerian and Lagrangian volume fluxes are identical. The Stokes drift increases in the presence of vegetation.

The finite vertical Stokes drift must be balanced by a gradient in the Eulerian, mean velocity field (return flow) in the limit of a steady solution. It was hypothesised that the Stokes velocity is established faster than the return flow, thus the vertical Stokes velocity is (partly) responsible for the mass flux needed to establish the mean wave-induced setup. This mean wave-induced setup is required to balance the gradient in the radiation stress tensor.

Further validation of the theory is needed. The validation material should preferably include data on (i) spatial variation in the surface elevation and (ii) orbital velocities over the height of the canopy for rigid stems. This will allow for a direct evaluation of the drag coefficients in a reduced velocity field.

References

Andrews, D.G., McIntyre, M.E., 1978. An exact theory of nonlinear waves on a Lagrangian-mean flow. J. Fluid Mech. 89, 609–646.

Asano, T., Deguchi, H., Kobayashi, N., 1992. Interaction between water waves and vegetation. Proc. Coast. Eng. Conf. VI, 2710–2723.

Bishop, C.T., Donelan, M.A., 1987. Measuring waves with pressure transducers. Coast. Eng. 11, 309–328.

Cao, H., Feng, W., Hu, Z., Suzuki, T., Stive, M.J.F., 2015. Numerical modeling of vegetation-induced dissipation using an extended mild-slope equation. Ocean Eng. 110, 258–269.

Dalrymple, R.A., Kirby, J.T., Hwang, P.A., 1984. Wave diffraction due to areas of energy dissipation. J. Waterw. Port Coast. Ocean Eng. ASCE 110 (1), 67–79.

Dalrymple, R.A., Losada, M.A., Martin, P.A., 1991. Reflection and transmission from porous structures under oblique wave attach. J. Fluid Mech. 224, 625–644.

Dean, R.G., Bender, C.J., 2006. Static wave setup with emphasis on damping effects by vegetation and bottom friction. Coast. Eng. 53, 149–156.

Deigaard, R., Fredsøe, J., 1989. Shear-stress distribution in dissipative water-waves. Coast. Eng. 13 (4), 357–378.

Dijkstra, J.T., Uittenbogaard, R.E., 2010. Modeling the interaction between flow and highly flexible aquatic vegetation. Water Resour. Res. 46 (W12547). (14 pages).

Döbken, J.W., 2015. Modeling the Interaction of Wave Hydrodynamics with Flexible Aquatic Vegetation. Delft University of Technology, Faculty of Civil Engineering and Geosciences. (June, Master thesis)

Fredsøe, J., Deigaard, R., 1992. Mechanics of coastal sediment transport. 1st edition, Advanced Series on Ocean Engineering, vol. 3. World Scientific.

Gu, Z., Wang, H., 1991. Gravity waves over porous bottoms. Coast. Eng. 15, 497–524.

Holthuijsen, L.H., 2007. Waves in Oceanic and Coastal Waters. 1st edition, Cambridge University Press.

Jacobsen, N.G., Van Gent, M.R.A., Wolters, G., 2015. Numerical analysis of the interaction of irregular waves with two dimensional permeable coastal structures. Coast. Eng. 102, 13–29.

Jensen, B., Jacobsen, N.G., Christensen, E.D., 2014. Investigations on the porous media equations and resistance coefficients for coastal structures. Coast. Eng. 84, 56–72.

Liu, P.L.-F., Dalrymple, R.A., 1984. The damping of gravity water-waves due to percolation. Coast. Eng. 8, 33–49.

Longuet-Higgins, M.S., Stewart, R.W., 1964. Radiation stresses in water waves — a physical discussion, with applications. Deep-Sea Res. 11 (4), 529–562.

Losada, I.J., Patterson, M.D., Losada, M.A., 1997. Harmonic generation past a submerged porous step. Coast. Eng. 31, 281–304.

Luhar, M., Coutu, S., Infantes, E., Fox, S., Nepf, H., 2010. Wave-induced velocities inside a model seagrass bed. J. Geophys. Res. 115 (C12005), 1–15.

Luhar, M., Nepf, H.M., 2016. Wave-induced dynamics of flexible blades. J. Fluids Struct. 61, 20–41.

Ma, G., Kirby, J.T., Su, S.F., Figlus, J., Shi, F., 2013. Numerical study of turbulence and wave damping induced by vegetation canopies. Coast. Eng. 80, 68–78.

Madsen, P.A., 1983. Wave reflection from a vertical permeable wave absorber. Coast. Eng. 7, 381–396.

Madsen, P.A., Schäffer, H.A., 1998. Higher-order Boussinesq-type equations for surface gravity waves: derivation and analysis. Philos. Trans. R. Soc. London, Ser. A 356 (1749), 3123–3184.

Mei, C.C., 1999. The applied dynamics of ocean surface waves, 1st edition. Advanced Series on Ocean Engineering. vol. 1. World Scientific.,

Mendez, F.J., Losada, I.J., 2004. An empirical model to estimate the propagation of random breaking and nonbreaking waves over vegetation fields. Coast. Eng. 51, 103–118.

Mendez, F.J., Losada, I.J., Dalrymple, R.A., Losada, M.A., 1998. Effects of wave reflection and dissipation on wave-induced second order magnitudes. Proc. Coast. Eng. Conf. I, 537–550.

Méndez, F.J., Losada, I.J., Losada, M.A., 1999. Hydrodynamics induced by wind waves in a vegetation field. J. Geophys. Res. 104 (C8), 18,383–18,396.

Philips, O.M., 1980. The Dynamics of the Upper Ocean. 2nd edition, Cambridge monographs on mechanics and applied mathematics, Press Syndicate of the University of Cambridge. (1st paperback edition)

Sánchez-González, J.F., Sánchez-Rojas, V., Memos, C.D., 2011. Wave attenuation due to *Posidonia oceanica* meadows. J. Hydraul. Res. 49 (4), 503–514.

Sollitt, C.K., Cross, R.H., 1972. Wave transmission through permeable breakwaters. Proc. Coast. Eng. Conf. III, 1827–1846.

Sumer, B.M., Fredsøe, J., 1999. Hydrodynamics around cylindrical structures. Advanced Series on Coastal Engineering, 1st edition, vol. 12. World Scientific.

Suzuki, T., Zijlema, M., Burger, B., Meijer, M.C., Narayan, S., 2011. Wave dissipation by vegetation with layer schematization in SWAN. Coast. Eng. 59, 64–71.

Uittenbogaard, R., Klopman, G., 2001. Numerical simulation of wave-current driven sediment transport. Proc. Coast. Dyn. I, 568–577.

Van Dyke, M., 2005. An Album of Fluid Motion. 1st edition, The Parabolic Press.

Van Gent, M.R.A., 1995. Porous flow through rubble mound material. J. Waterw. Port Coast. Ocean Eng. ASCE 121 (3), 176–181.

Van Rooijen, A.A., McCall, R.T., Thiel de Vries, J.S.M., Van, Van Dongeren, A.R., Reniers, A.J.H.M., Roelvink, J.A., 2016. J. Geophys. Res. Oceans http://dx.doi.org/10.1002/2015JC011392.

Wu, W., Ozeren, Y., Chen, Q., Holland, M., Ding, Y., Kuiry, S.N., Zhang, M., Jadhav, R., Chatagnier, J., Chen, Y., Gordji, L., 2011. Investigation of surge and wave reduction by vegetation. Tech. Rep. Phase I report for SERRI project no. 80037. National Center for Computational Hydroscience and Engineering; The University of Mississippi.